The Pressure Dependence of the OH Radical Yield from Ozone−Alkene Reactions

Jill D. Fenske,[†] Alam S. Hasson,[‡] Suzanne E. Paulson,*[,‡] Keith T. Kuwata,[§] Andy Ho,[§] and K. N. Houk*[,§]

Departments of Chemical Engineering, Atmospheric Science, and Chemistry and Biochemistry, University of California at Los Angeles, Los Angeles, California 90095-1565

Received: March 23, 2000; In Final Form: June 20, 2000

The OH radical is the key oxidizing agent in the troposphere, and ozone−alkene reactions appear to be a significant and sometimes dominant source of new HO_x radicals in urban and rural air. In this work, we report the first study of the pressure dependence of the OH radical yield for the ozonolysis of ethene, propene, 1-butene, *trans*-2-butene, and 2,3-dimethyl-2-butene over the range 20−760 Torr and of *trans*-3-hexene and cyclopentene over the range 200−760 Torr. Low-pressure experiments were performed in a long-path evacuable FTIR cell or a steady-state flow-tube reactor in series with a gas chromatograph/flame ionization detector and FTIR cell. We have also investigated the effect of adding SF_6 at atmospheric pressure for ethene, 1-butene, and *trans*-2-butene, in a collapsible Teflon chamber. OH formation increased almost 3-fold for ethene at low pressures, from 0.22 ± 0.06 at 760 Torr to 0.61 ± 0.18 at 20 Torr, and increased somewhat for propene from 0.33 ± 0.07 at 760 Torr to 0.46 ± 0.11 at 20 Torr. A pressure dependence of the OH formation yield was not observed for 1-butene, *trans*-2-butene, 2,3-dimethyl-2-butene, *trans*-3-hexene, or cyclopentene over the ranges studied. Density functional theory calculations at the B3LYP/6-31G(d,p) level are presented to aid in understanding the trends observed. They lead to the proposal that the formation of a hydroperoxide via a diradical pathway can compete with the formation of the carbonyl oxide for the ethene primary ozonide.

Introduction

The hydroxyl radical is a powerful oxidant in the atmosphere. Throughout the troposphere, the dominant source of OH in the atmosphere is generally considered to be ozone photolysis. However, several recent studies show that the ozone reaction with alkenes leads to the direct formation of OH radicals,[1−6] with the amount depending on the alkene. In addition to OH radicals, ozone−alkene reactions also likely produce organic peroxy radicals (RO_2).[1,7] In the boundary layer, HO_x (═OH, RO_2, HO_2) production from ozone−alkene reactions may be a significant, and sometimes dominant, contribution to the total HO_x production during both day and night.[8]

The reactions of ozone with alkenes have been the subject of many excellent studies over the past four decades, yet a clear understanding of the mechanisms, and a resulting predictive capability, is still elusive. The pressure dependence of product formation has the potential to provide insights into several aspects of the mechanism. To date, only a few measurements of OH formation at pressures other than 1 atm have been reported. Donahue et al.[5] used laser-induced fluorescence to measure OH directly from ozonolysis of ethene, isoprene, *trans*-2-butene, and 2,3-dimethyl-2-butene at 4−5.5 Torr. Their low-pressure experiments with ethene and isoprene give much larger OH yields than the atmospheric pressure measurements: 0.42 vs 0.18 for ethene at 5.5 Torr and 1 atm,[9] respectively; 0.5 vs 0.25 for isoprene at 4 Torr and 1 atm,[9] respectively. The reported uncertainty for the low-pressure measurements is ±50%; thus the low and atmospheric pressure values are actually in agreement within the mutual uncertainties. Donahue et al.'s[5] values at low pressure for *trans*-2-butene (0.6) and 2,3-dimethyl-2-butene (0.7), on the other hand, are in much closer agreement with the previously measured atmospheric pressure values of about 0.65 and 0.8, respectively. Thomas et al.[10] performed studies on the dependence of yields of stable products with pressure (at 770, 77, and 7.5 Torr) for the reaction of ozone with ethene. They observed no pressure dependence above 77 Torr; below 77 Torr, an increase in CO and CO_2 yields and a decrease in the formaldehyde yield were observed.

In this work, we report the first study of the pressure dependence of the OH radical yield for ethene, propene, 1-butene, *trans*-2-butene, and 2,3-dimethyl-2-butene over the range 20−760 Torr and for *trans*-3-hexene and cyclopentene over the range 200−760 Torr. Measurements were made using a gas chromatograph/flame ionization detector (GC/FID) and long-path Fourier transform infrared (FTIR) spectroscopy and the small-ratio relative-rate technique.[11] To investigate the potential dependence of OH formation on pressure above 1 atm, we also performed experiments with 20−100% SF_6 in the matrix gas at 1 atm in air for ethene, 1-butene, and *trans*-2-butene. In addition, estimates of the pressure dependence of CO and aldehyde yields for ethene and propene are reported. Density functional theory calculations are also presented for ethene and propene in an effort to provide a theoretical interpretation for the results.

Mechanism of Ozonolysis

The reaction of ozone with alkenes occurs via cycloaddition of ozone to the double bond. The resulting five-membered ring is thought to decompose by one of two mechanisms: homolysis of an O−O bond to form a diradical species (R1b)[12,13] or concerted O−O and C−O bond breakage to form a carbonyl

* Authors to whom correspondence should be addressed.
[†] Department of Chemical Engineering.
[‡] Department of Atmospheric Science.
[§] Department of Chemistry and Biochemistry.

10.1021/jp001100u CCC: $19.00
Published on Web 07/29/2000

TABLE 1: Measured OH Yields from the Ozone Reaction with Several Alkenes

alkene	pressure (Torr)	OH yield[a] (this work)	pressure (Torr)	literature	ref
ethene	760, 100% SF_6	0.06 ± 0.01			
	760, 50% SF_6	0.12 ± 0.05			
	760, 35% SF_6	0.15 ± 0.03			
	760, 20% SF_6	0.21 ± 0.04			
	760	0.22 ± 0.06	760	0.18 ± 0.06[c]	this lab[9]
			760	0.12 (+0.06, −0.04)	15
			760	0.14 ± 0.04	45
			760	0.08 ± 0.01	46
	750[b]	0.20 ± 0.05	750	0.20 ± 0.02	47
	400	0.26 ± 0.06			
	200	0.29 ± 0.06			
	100	0.32 ± 0.09			
	50[b]	0.50 ± 0.15			
	20	0.61 ± 0.18	5.5	0.42 ± 0.21	5
propene	760	0.33 ± 0.07	760	0.35 ± 0.07[c]	this lab[9]
			760	0.18 ± 0.04	46
			760	0.33 (+0.16, −0.11)	15
			760	0.32 ± 0.08	45
			760	0.34 ± 0.06	48
	713[b]	0.37 ± 0.08			
	600	0.31 ± 0.06			
	400	0.33 ± 0.08			
	238[b]	0.42 ± 0.10			
	200	0.34 ± 0.08			
	108[b]	0.50 ± 0.08			
	85	0.46 ± 0.11			
	60	0.49 ± 0.12			
	58[b]	0.50 ± 0.14			
	20	0.46 ± 0.11			
1-butene	760, 40% SF_6	0.24 ± 0.05			
	760, 30% SF_6	0.27 ± 0.06	760	0.41 (+0.2, −0.13)	15
	760	0.23 ± 0.04	760	0.24 ± 0.05	this lab[16]
	60	0.30 ± 0.08			
	20	0.26 ± 0.07			
trans-2-butene	760, 70% SF_6	0.63 ± 0.13			
	760, 50% SF_6	0.55 ± 0.11	760	0.65 ± 0.13[c]	this lab[49]
	760, 30% SF_6	0.62 ± 0.13	760	0.24 ± 0.02	46
	760	0.67 ± 0.19	760	0.64 (+0.32, −0.21)	15
	760	0.56 ± 0.12	760	0.54 ± 0.13	50
	200	0.62 ± 0.14	5.5	0.60 ± 0.30	5
	60	0.59 ± 0.17	4.5	0.72 ± 0.36	5
2,3-dimethyl-2-butene	760	0.99 ± 0.18	760	1.0 ± 0.2	15
			760	0.70 ± 0.10	1
			760	1.0 ± 0.2	this lab[49]
			760	0.80 ± 0.12	51
			760	0.36 ± 0.02	46
			760	0.89 ± 0.22	45
	60	0.85 ± 0.22			
	20	1.04 ± 0.26	4.3	0.70 ± 0.35	5
trans-3-hexene	760	0.62 ± 0.11	760	0.47 ± 0.07	this lab[49]
	760	0.46 ± 0.17			
	350	0.46 ± 0.17			
	200	0.49 ± 0.10			
cyclopentene	760	0.58 ± 0.16	760	0.62 ± 0.15[c]	this lab[52]
	200	0.59 ± 0.12			

[a] Uncertainties reported here reflect experimental and systematic uncertainties (see Table 2 and text). [b] Value from experiments performed in NCAR cell. [c] Value from smog chamber experiments reported in corresponding reference.

product and a carbonyl oxide (R1a) (Criegee mechanism).[14] For ethene:

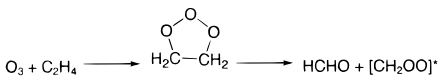

(R1a)

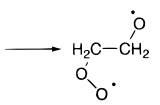

(R1b)

The Criegee mechanism is currently thought to be the dominant decomposition pathway for the primary ozonide.[15] Most of the initial carbonyl oxide is vibrationally excited and may presumably either decompose or be collisionally thermalized by the surrounding gas:[14,15]

$$[CH_2OO]^* \xrightarrow{M} CH_2OO \quad \text{(R2a)}$$

$$\xrightarrow{M} HC(O)OH \quad \text{(R2b)}$$

$$\rightarrow 2H + CO_2 \quad \text{(R2c)}$$

$$\rightarrow H_2O + CO \quad \text{(R2d)}$$

$$\rightarrow CO_2 + H_2 \quad \text{(R2e)}$$

$$\rightarrow OH + HCO \quad \text{(R2f)}$$

$$HCO \rightarrow H + CO \qquad (R3)$$

OH radical formation has been measured by several groups, with values ranging from 0.08 to about 1, depending on the alkene (see Table 1 or Paulson, Chung, and Hasson[16]). At very high O_3 concentrations, some formation of OH radicals may arise from subsequent reactions of the H atoms formed in R2c and R3.

$$H + O_2 \xrightarrow{M} HO_2 \qquad (R4)$$

$$HO_2 + O_3 \rightarrow OH + 2O_2 \qquad (R5)$$

$$H + O_3 \rightarrow OH + O_2 \qquad (R6)$$

This source is small for the experiments described here and negligible in the atmosphere.

A few studies have investigated the pressure dependence of the thermalized carbonyl oxide yield. For ethene, the yield of thermalized carbonyl oxide decreases with pressure, as might be expected, but does not approach zero at very low pressures.[17] Hatakeyama et al.[18] measured an atmospheric pressure yield of thermalized carbonyl oxide of 0.39 ± 0.05 and found that the yield begins a sharp decrease at 600 Torr, reaching 0.20 at 10 Torr. This result led them to conclude that 20% of the carbonyl oxide from the ozone−ethene reaction is formed already thermalized. For *trans*-2-butene, however, the thermalized carbonyl oxide yield begins to decline at approximately 250 Torr, approaching zero at low pressures (<10 Torr), indicating that none of the carbonyl oxide from the reaction of ozone with *trans*-2-butene is formed initially cold. Olzmann et al.[19] used master-equation analysis and statistical rate theory to model the OH radical and thermalized carbonyl oxide yields from ozone reactions with ethene and 2,3-dimethyl-2-butene. They predict no pressure dependence for ethene and a small pressure dependence for 2,3-dimethyl-2-butene for both OH and thermalized carbonyl oxide formation. This prediction arises from calculations indicating that energy transfer is competitive with isomerization and decomposition for 2,3-dimethyl-2-butene but not for ethene. There is a weak anticorrelation between the formation of OH radicals and formation of thermalized carbonyl oxides.[16] The correlation is most likely weak because of the additional isomerization pathways open to the carbonyl oxides other than OH formation and collisional deactivation.

Early theoretical studies of gas-phase ozonolysis focused on the reactions of diradicals formed by homolysis of an O−O bond in the primary ozonide.[12,13,20] O'Neal and Blumstein[20] suggested that a 1,4-hydrogen shift within an ozonide diradical would lead to a hydroperoxide that could subsequently decompose to afford OH radicals.

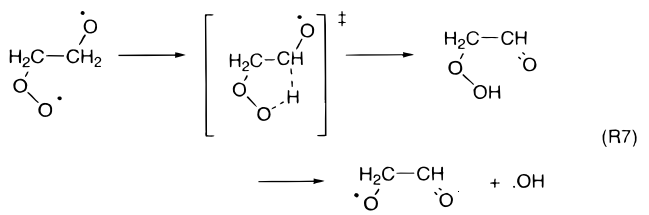

(R7)

This pathway was also considered by Goddard and co-workers in their early GVB-CI calculations.[12,13] Later, Cremer[21] performed extensive HF and MP2 calculations on the pseudorotation of primary and secondary ozonides, assuming a concerted decomposition of the primary ozonides.

In 1991, Dewar et al.[22] reported AM1 transition states for the ozonolysis of ethene, propene, and *cis*- and *trans*-2-butene. They predicted that ozonolysis proceeds exclusively by concerted pathways and that the stereochemistry of the reaction was controlled by the cycloreversion of the primary ozonide. Subsequent ab initio and density functional studies by Anglada et al.[23] and by Cremer and co-workers[7,24] focused on the unimolecular reactions of the Criegee intermediate that results from a concerted cycloreversion of the primary ozonide.

Anglada et al.[25] have recently revisited the possibility that the hydroperoxide (as in Figure 7, **9**) could be an alternative source of OH radicals. Using CCSD(T)/6-311G(2d,2p) and CASPT2(6,6)/6-311G(2d,2p) calculations, they predict that the concerted cycloreversion transition state is lowest in energy and that the 1,4-hydrogen shift transition state is 4.1−7.4 kcal/mol higher in energy. Their results suggest that the hydroperoxide could play at most a minor role in gas-phase ethene ozonolysis.

OH formation via channel R2f has been proposed to proceed by H migration and subsequent decomposition. CCSD(T) calculations by Gutbrod et al. indicate that, for ethene, this pathway has a fairly high activation barrier (31 kcal/mol) compared to dioxirane formation (R9), which has an activation barrier of about 18 kcal/mol.[24]

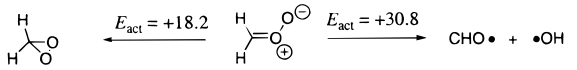

These activation barriers are not consistent with OH formation from ethene ozonolysis of 12−22% at atmospheric pressure (Table 1).

Niki et al.[1] postulated that, for larger alkenes, OH formation occurs via a vibrationally excited unsaturated vinyl hydroperoxide, as in R8c. For *trans*-2-butene:

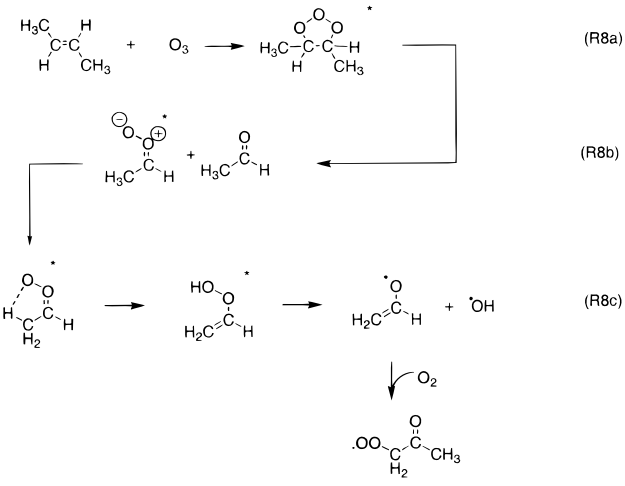

The carbonyl oxides formed in R8b may have either an anti or syn configuration:

Recent MRDCI and B3LYP calculations have shown that the activation energy barrier for interconversion between these two carbonyl oxide isomers is about 30 kcal/mol.[23,52] The B3LYP activation energy for the vinyl hydroperoxide channel (R8c), available only to the syn isomer, is 15 kcal/mol for CH_3CHOO.[7]

B3LYP calculations indicate that formation of dioxirane (R9) requires 24 and 17 kcal/mol for syn and anti CH_3CHOO, respectively.

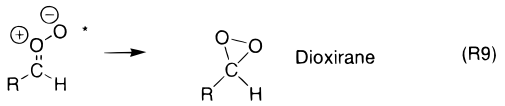

The B3LYP predictions for the dimethyl carbonyl oxide are similar to those for CH_3CHOO, with the vinyl hydroperoxide OH formation channel favored over the dioxirane channel (14 and 21 kcal/mol, respectively).[7]

Technique for Measuring OH Yields

In this study, we use the small-ratio, relative-rate technique, which has been discussed in detail elsewhere.[11] When the tracer is present in low concentrations (i.e. <10% of the alkene concentration), most of the OH reacts with the alkene rather than the tracer. Under these conditions, up to 30% of the tracer may be consumed.

$$O_3 + \text{alkene} \xrightarrow{k_{O_3}} y_{OH}OH + y_{OH}RO_2 + \text{other products} \quad \text{(R10)}$$

$$OH + \text{alkene} + M \xrightarrow{k_A} RO_2 + M \quad \text{(R11)}$$

$$OH + \text{tracer} + M \xrightarrow{k_{Tr}} RO_2 + M \quad \text{(R12)}$$

The tracers used in this study were 1,3,5-trimethylbenzene (TMB) and *m*-xylene (XYL).

An OH yield can be derived from an analytical expression obtained from solving eqs R10−R12, but the most accurate way to calculate the OH yield is by solving the ordinary differential equations that describe the complete system, including the reactions of the products, wall losses, and so forth. The analytical and numerical solutions generally fall within 20% of one another.[11] The data in this study were analyzed numerically. The OH yield for each experiment was determined using a least-squares fitting procedure. An Excel macro was used to evaluate $\Sigma(y_e - y_m)^2$ for each experimental data set where y_e and y_m are the percentage of tracer reacted in the experiment and model respectively (i.e., the *y* values in Figure 1). This process was repeated for model runs with different OH yields until this quantity had been minimized.

The chemistry of each reaction system was described in the following way: The OH and O_3 rate constants with the hydrocarbons are from Atkinson,[15,26] except for the OH−TMB rate constant, which is from Kramp and Paulson.[27] A detailed explanation of the chemistry used in the propene model can be found in Paulson et al.,[11] and the other alkenes were modeled analogously. The ozone reaction with alkenes is assumed to generate RO_2 radicals together with OH radicals (R10). These RO_2 radicals presumably have a β-carbonyl group and thus were assumed to react with rates comparable to primary, secondary, or tertiary β-hydroxy alkoxy radicals, depending on the alkene. The RO_2 chemistry is from Jenkin and Hayman[28] and Lightfoot et al.[29] The reactions of common products, RO_2 radicals, and tracers are listed in detail in Paulson et al.[11] A few of the reactions taking place in the experiments described here are pressure-dependent and potentially introduce additional uncertainties (as discussed below).

The calculated OH yields are most sensitive to the OH rate constant of the tracer. In this analysis, TMB−OH and XYL−OH rate constants of $(57.3 \pm 5.3) \times 10^{-12}$ cm^3 molec^{-1} s^{-1} and $(22.0 \pm 2.7) \times 10^{-12}$ cm^3 molec^{-1} s^{-1}, respectively, were assumed.[27] Paulson et al.[11] showed that any uncertainty in the tracer−OH rate constant directly translates to the uncertainty in the OH yield. The yields are not particularly sensitive to assumptions made about the products. A detailed sensitivity analysis indicated that the uncertainty in the products introduces an uncertainty in the OH yield of 5−6% for propene.[11]

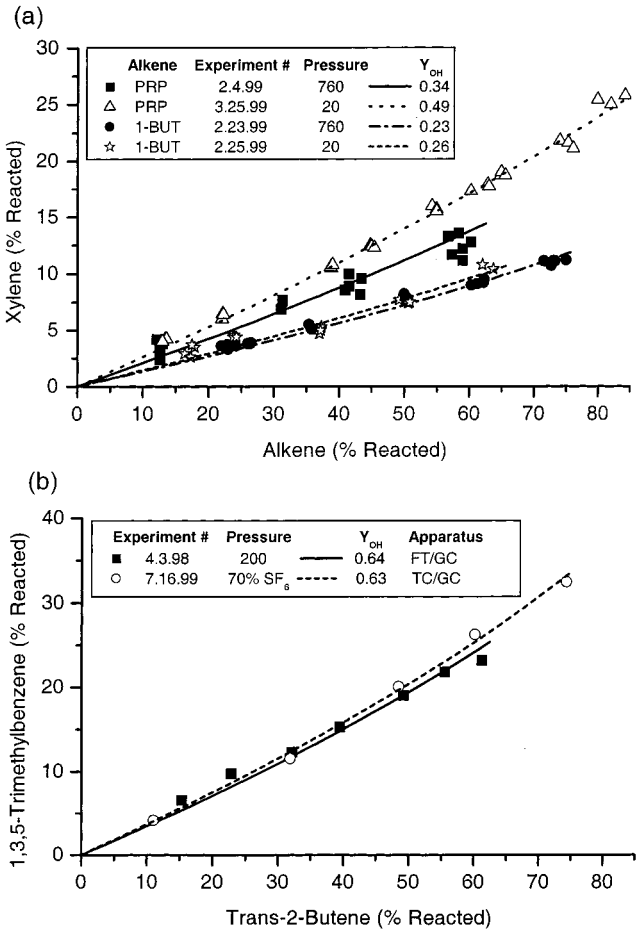

Figure 1. Representative tracer and alkene data for propene, 1-butene and *trans*-2-butene (symbols). The lines represent the best-fit model curve for each experiment. Panel (a) shows data from minimum (20 Torr, triangles and stars) and maximum (760 Torr, squares and circles) pressures, performed in the UCLA FTIR cell and using XYL as tracer. Panel (b) shows *trans*-2-butene data from the flow tube (squares) and the collapsible Teflon chamber (circles), the latter performed in 70% SF_6/30% air.

Some of the HO_2, CO, ethene, and propene reactions are pressure-dependent.[30] The CO−OH reaction is not significant because the alkene and tracer scavenge most of the OH formed. As the pressure is decreased, the rate coefficient for the HO_2 self-reaction decreases, opening the possibility of an increase in the reaction of HO_2 with O_3. Calculations indicate that setting all other reactions of HO_2 to zero so that HO_2 reacts only with O_3 has a negligible effect on the calculated OH yield. Further, increasing the O_3 concentration in the model to 2.6×10^{14} molec cm^{-3} decreased the calculated OH yield by 18% (with all HO_2 chemistry included). This is comparable to the O_3 concentration in the O_2/O_3 stream added to the FTIR cell in these experiments (at 20 Torr). The high concentration in the O_3/O_2 stream is not expected to have a significant impact, as complete mixing is expected to occur in less than 10 s (on the basis of wall-loss measurements and visual observation of brown NO_2 formation during design of the injector). The rate coefficient for ethene reaction with OH is somewhat pressure-dependent, with values

of $(6 \pm 2) \times 10^{-12}$ and $(8.5 \pm 0.6) \times 10^{-12}$ cm^3 molec^{-1} s^{-1} for 20 Torr and atmospheric pressure, respectively.[31] For ethene, a 35% increase or decrease in the ethene−OH rate coefficient (the recommended uncertainty for this value at 20 Torr)[32] resulted in a 15% change in the OH yield in the same direction. The propene reaction with OH is nearly independent of pressure; less than a 5% difference between the rate constant at atmospheric pressure (2.6×10^{-11} cm^3 molec^{-1} s^{-1}) and that at 20 Torr has been reported,[31] which falls within the recommended uncertainty of the rate constant at atmospheric pressure.[32] The rate constants for reactions of OH with alkenes with four or more carbon atoms reach their high-pressure limits at less than 20 Torr.[33]

In summary, the chemical model carries with it a systematic uncertainty at atmospheric pressure of about ±15%. At low pressures (<100 Torr), this systematic uncertainty rises to ±23% for compounds with three or more carbons, because of uncertainties in the pressure dependence of secondary reactions. For ethene, the uncertainty is higher below 100 Torr; about ±28%, because of the uncertainty introduced by the low-pressure measurements of the rate coefficient for OH radical reaction with ethene. The above-described systematic uncertainties in the calculated OH yield from the chemical model should thus be taken into account when the OH yields at various pressures are compared.

Experimental Description

Three experimental apparatuses were used in this study: a 250-L collapsible Teflon chamber operated at atmospheric pressure, a variable-pressure flow-tube (both with GC/FID detection), and a 50-L evacuable multireflection FTIR cell. The Teflon chamber was used to obtain atmospheric pressure OH yields for comparison with results from the flow tube and is described in detail elsewhere.[11] Briefly, it consists of a pillow-shaped 200−250-L Teflon chamber held at 296 ± 2 K and placed in a dark enclosure. The chamber was equipped with a Teflon tube "injector" (a length of $^1/_4$ in. o.d. Teflon tubing with holes at intervals) to reduce sample mixing time. A stream of zero air (Thermo Environmental Zero-Air Generator, Model 111) flushed evaporated liquid hydrocarbons into the chamber as it filled. Ozone was generated in aliquots by flowing pure O_2 through a mercury lamp ozone generator (JeLight PS-3000-30).

The flow-tube apparatus consists of a 2 cm i.d. × 2 m glass tube equipped with stainless steel endplates that provide connection ports for the transfer tubing. Separate inlet ports were used to introduce the hydrocarbons and the synthetic air; a small "turbulizer" (fan-shaped piece of Teflon) provided thorough mixing as soon as the gases entered the flow tube. The temperature during the experiments was 296 ± 2 K, and the pressure was monitored at the end of the flow tube with a Baratron (Model 127AA) 1−1000-Torr pressure gauge. The hydrocarbon bulbs (~12 L) were prepared on a vacuum line and contained a high concentration (>1×10^{17} molec cm^{-3}) of the hydrocarbons used for each experiment. The liquid hydrocarbons were evaporated into the vacuum line to a selected pressure, and then the bulbs were pressurized to ~1100 Torr with nitrogen. Flow controllers (Unit Instruments Model 8100) provided specified quantities of alkene and tracer with a stated uncertainty of ±1%. For the flow-tube experiments, the tracer-to-alkene ratio was held at about 0.05. The carrier gas was a synthetic mix of nitrogen and oxygen (80% and 20%, respectively) (Lehner-Martin, liquid grade), the total flow rate of which was also determined by a flow controller (Unit Instruments Model 3020A). The ozone was generated by flowing the synthetic air mixture through a mercury lamp ozone generator (mentioned above) at atmospheric pressure, or at low pressure by passing a separate flow of pure oxygen through the ozone generator and bleeding this into the synthetic air line with a needle valve. The ranges of O_3 concentrations obtained in the flow tube were $(1.2-47) \times 10^{13}$ molec cm^{-3} at 760 Torr using synthetic air and $(6.5-30) \times 10^{13}$ molec cm^{-3} at 200 Torr using pure oxygen. Low pressures were maintained by balancing the flows with a vacuum pump.

The flow tube operated in the developing flow regime, and the velocity profile was flat throughout the length of the tube. A flat velocity profile ensures that, across any radial section of the flow tube, all components have been exposed to the same reaction time and concentrations. The flat velocity profile was verified using a hot-wire anemometer (TSI 1053B) to measure the velocity of air as a function of radial position across the tube (Fenske et al., unpublished work). The radial velocity measurements were performed using an identical flow tube with openings every 10 in. for insertion of the anemometer probe. All openings not being used during a particular measurement were sealed, and the anemometer probe was mounted through a rubber stopcock equipped with O-rings to prevent leaks around the probe body. The range of total flow rates used in the flow tube for this study was 1.5−3 L/min; the hydrocarbon flow rates were varied from 2 to 15 mL/min. The residence times in these experiments were 13−25 s (corresponding to Reynolds numbers of 105−211) and were selected to ensure that greater than 95% of the ozone would react by the end of the tube. The pressure drop across the flow tube at these flow rates was negligible (~1 mTorr). A study of hydrocarbon and ozone concentrations at the beginning and end of the tube showed that wall losses for these compounds were negligible. Calculations using the model described above showed that this experiment is insensitive to wall losses of OH radicals, as the lifetime of OH radicals with respect to reaction is $\leq 10^{-5}$ s.

Experiments in the flow tube were conducted as follows: The hydrocarbon and air flows were set to give the desired residence time and hydrocarbon concentrations, and the hydrocarbon concentrations were monitored by GC/FID to ensure that steady state had been reached. Steady state was usually established in 20 min. The ozone generator was then turned on, and the change in hydrocarbon concentrations was monitored by GC/FID. The ozone concentration was varied (in random order) to obtain each data point.

A gas chromatograph/flame ionization detector (GC/FID) (Hewlett-Packard 5890), equipped with a computer-controlled 2-mL gas sampling valve and either a 30 m × 3 μm × 0.53 mm i.d. DB-624 or a 30 m × 3 μm × 0.32 mm i.d. DB-1 column (J & W), monitored the hydrocarbon concentrations throughout the experiments. The GC was calibrated daily with a cyclohexane standard (Scott Specialty Gases), and the concentration of each hydrocarbon was determined using its carbon number to calculate the FID response normalized to the cyclohexane calibration.

The FTIR long-path cell apparatus consists of a 50-L glass cell, with a 1.5-m base path length (Infrared Analysis). The FTIR spectrometer (Bruker Vector 22) was equipped with a mercury−cadmium−telluride detector (Belov B18N-40); the optics were purged with dry nitrogen. An injector, which consisted of a 120-cm length of Teflon tubing with a Silcosteel insert (Restek), drilled with holes from 0.79 to 7.9 mm in diameter at 10-cm intervals, introduced the gases into the long-path cell. The optimal hole sizes for the injector were selected by flowing NO

into air through the injector. Through the observation of (brown) NO_2 formation, the hole sizes were adjusted to provide thorough and instantaneous mixing. The injector reduces the mixing time within the cell significantly. This study used a 90-m path length, 0.5-cm^{-1} resolution, and 64 scans per spectrum. A Baratron (127AA, 1−1000 Torr) and a thermocouple gauge (Veeco TG-70, 1−1000 mTorr) monitored the pressure. Hydrocarbon wall losses in the FTIR cell were measured by monitoring losses for concentrations comparable to the experimental conditions. For the alkenes, the wall losses were negligible; wall losses for the tracers were $\leq 10^{-6}$ s^{-1} and were included in the model. A very similar apparatus was used in a small set of experiments performed at NCAR (National Center for Atmospheric Research); the NCAR cell has been described in more detail elsewhere.[34]

The FTIR cell experiments were carried out in the following manner: After pure oxygen was added to the cell to 20% of the final pressure, a calibrated volume was pressurized with each hydrocarbon, and these were swept into the cell with boil-off from a liquid nitrogen cylinder. Once the hydrocarbons were added, the cell was pressurized to within a few percent of the final pressure, and the initial concentrations were measured by FTIR. At NCAR, aliquots of an ozone/oxygen mixture were swept into the cell to reach the desired final pressure. At UCLA, ozone was generated by flowing pure oxygen through a mercury lamp ozone generator (JeLight PS-3000-30) and was added to the cell directly through a needle valve. A second measurement with the FTIR gave the amount of tracer and alkene reacted away, so that each fill of the cell provided one, or at most two, data points. The run-to-run reproducibility of the initial concentrations of tracer and alkene were within ±10% and ±5%, respectively, and the initial tracer-to-alkene ratio was 0.11 ± 0.02. Because this is a relative measurement, absolute differences in the initial concentrations from run to run are unimportant as long as the ratio of tracer to alkene does not change significantly. The IR bands used were as follows: 1,3,5-trimethylbenzene, 820−850 cm^{-1}; *m*-xylene, 740−800 cm^{-1}; 2,3-dimethyl-2-butene, 1140−1190 cm^{-1}; *trans*-2-butene, 920−1000 cm^{-1}; 1-butene, 900−950 cm^{-1}; propene, 850−920 cm^{-1}; ethene, 850−1100 cm^{-1}; formaldehyde, 2600−2840 cm^{-1}; and propionaldehyde, 2650−2750 cm^{-1}.

To investigate the potential dependence of OH formation on pressure above 1 atm, we also performed experiments with 20−100% SF_6 (Mattheson) in the matrix gas at 1 atm in air for ethene, 1-butene, and trans-2-butene. These experiments were carried out in both the Teflon chamber and the FTIR cell.

The hydrocarbons (Aldrich) were 99% pure or better (except for 1,3,5-trimethylbenzene, which was 98% pure) and were used as received.

Theoretical Methods

The geometries and energies of minima and transition structures were determined using density functional theory, employing the Becke3LYP hybrid functional[35] and the 6-31G-(d,p) basis set[36,37] [B3LYP/6-31G(d,p)]. Species with unpaired electrons were treated with unrestricted Becke3LYP (UB3LYP) theory; open-shell singlets were described with wave functions of broken spin symmetry. All energies reported included corrections for zero-point energies derived from the (U)B3LYP/6-31G(d,p) harmonic frequencies scaled by a factor of 0.963. All results reported here were obtained with the Gaussian 94[38] and Gaussian 98[39] suites of programs.

Results

Representative data from the three apparatuses and 6 of the 71 experiments are shown in Figure 1. Calculated best-fit OH yields for each experiment are shown, together with uncertainties, in Table 2. Experimental uncertainties were determined by calculating the OH yield corresponding to the farthest outlying data points in each experiment. These OH yields carry an additional systematic uncertainty, which increases from ±15% at atmospheric pressure to ±28% below 100 Torr for ethene (see above) and ±23% below 100 Torr for all other compounds studied. Data are plotted as percent of tracer reacted vs percent of alkene reacted; also shown are lines indicating model calculations for best-fit OH yields. Panel a shows propene and 1-butene data at 760 and 20 Torr, using XYL as the tracer, performed in the UCLA FTIR cell. The propene data clearly show a pressure dependence, whereas the 1-butene data do not. Panel b shows *trans*-2-butene data using TMB as the tracer, showing that more tracer is consumed than in XYL experiments (Panel a). Experiment 4.3.98 was performed in the flow tube (solid squares), whereas experiment 7.16.99 (open circles) was performed in the Teflon chamber, filled with 70% SF_6/30% air. These data do not indicate any pressure dependence for *trans*-2-butene. Additional data are available from the authors.

The OH formation yields from the O_3 reaction with ethene, propene, 1-butene, *trans*-2-butene, *trans*-3-hexene, 2,3-dimethyl-2-butene, and cyclopentene are summarized in Table 1. Table 1 also shows averaged values (from Table 2) for the OH yields at each pressure and for each experimental apparatus, together with the estimated uncertainties in the data. Results for ethene, propene, 1-butene, and *trans*-2-butene are plotted as a function of pressure and SF_6 content in Figures 2−4; for conciseness, OH yields for 2,3-dimethyl-2-butene, *trans*-3-hexene, and cyclopentene, which were found to be independent of pressure, are not plotted.

The OH radical yield from the ozone reaction with ethene (Figure 2) has a strong pressure dependence below 100 Torr, increasing from 0.21 ± 0.04 at atmospheric pressure to 0.32 ± 0.09 at 100 Torr and then sharply increasing to 0.61 ± 0.18 at 20 Torr. The OH yield also decreases with increasing SF_6 content, reaching a yield of 0.06 ± 0.01 at 100% SF_6 bath gas. Miller and Barker found SF_6 to be approximately 10 times more effective at collisional energy removal from pyrazine than N_2;[42] thus, the experiments with added SF_6 may simulate pressures greater than 760 Torr. The OH yield does not appear to reach a limiting value at the lowest pressure used in this study. The only other low-pressure measurement of OH formation from ethene was 0.42 ± 0.21 at 5.5 Torr, performed by Donahue et al.[5] The lowest pressure we could study was 20 Torr, where we measured an OH yield of 0.61 ± 0.18. The values fall within their mutual uncertainties, but Donahue et al.'s[5] measurement does not seem to support the notion that OH yields continue to increase at pressures below 20 Torr.

The OH yield from the ozonolysis of propene has a weaker pressure dependence (Figure 3), rising from 0.33 ± 0.07 at atmospheric pressure to 0.46 ± 0.11 at 85 Torr. For propene, the OH yield appears to reach a limiting value below 100 Torr, remaining at about 0.48 for pressures down to 20 Torr. The OH yields as a function of pressure for the ozone reactions with 1-butene, *trans*-2-butene, *trans*-3-hexene, 2,3-dimethyl-2-butene, and cyclopentene are summarized in Table 1. The low end of the pressure ranges were 20 Torr for 1-butene and 2,3-dimethyl-2-butene, 60 Torr for *trans*-2-butene, and 200 Torr for *trans*-3-hexene and cyclopentene. In addition, measurements of OH yields from 1-butene and *trans*-2-butene ozonolysis were made

TABLE 2: Summary of Initial Conditions and OH Yields for Each Experiment

alkene	tracer	expt #	*P* (Torr)	type[a]	$[A]_o$[b] (molec/cm^3)	$[T]_o$[c] (molec/cm^3)	Yoh[d] model
ethene	TMB	7.26.99	>760,[e] 100% SF_6	TC/GC	3.22E+14	1.35E+13	0.06 ± 0.01
	TMB	7.6.99	>760,[e] 50% SF_6	TC/GC	2.76E+14	4.50E+12	0.14 ± 0.04
	XYL	3.26.99		FTIR/GC	6.10E+14	8.51E+13	0.11 ± 0.02
	TMB	7.8.99	>760,[e] 35% SF_6	TC/GC	2.43E+14	4.28E+12	0.15 ± 0.02
	TMB	7.7.99	>760,[e] 20% SF_6	TC/GC	2.23E+14	7.13E+12	0.21 ± 0.03
	XYL	3.16.99A	760	FTIR	7.33E+14	8.34E+13	0.22 ± 0.05
	TMB	NCAR750	750		2.28E+15	2.29E+14	0.20 ± 0.04
	XYL	3.16.99B	400	FTIR	7.43E+14	8.79E+13	0.26 ± 0.04
	XYL	3.15.99	200	FTIR	6.24E+14	8.35E+13	0.29 ± 0.04
	XYL	3.10.99	100	FTIR	5.70E+14	7.35E+13	0.32 ± 0.03
	TMB	NCAR50	50	FTIR	2.82E+15	2.80E+14	0.50 ± 0.05
	XYL	3.9.99	20	FTIR	2.63E+14	6.86E+13	0.61 ± 0.05
propene	TMB	NCAR713	713	FTIR	2.72E+15	2.84E+14	0.37 ± 0.06
	TMB	NCAR238	238	FTIR	2.08E+15	2.11E+14	0.42 ± 0.08
	TMB	NCAR108	108	FTIR	2.25E+15	2.24E+14	0.50 ± 0.03
	TMB	NCAR58	58	FTIR	2.57E+15	2.57E+14	0.50 ± 0.08
	XYL	2.4.99	760	FTIR	6.69E+14	6.20E+13	0.34 ± 0.05
		2.5.99			7.04E+14	6.96E+13	0.32 ± 0.05
	XYL	3.4.99	600	FTIR	7.42E+14	8.78E+13	0.31 ± 0.04
	XYL	3.17.99	400	FTIR	7.08E+14	8.04E+13	0.33 ± 0.06
	XYL	3.3.99	200	FTIR	7.32E+14	7.64E+13	0.34 ± 0.06
	XYL	3.2.99	85	FTIR	7.46E+14	8.53E+13	0.46 ± 0.03
	XYL	2.16.99	60	FTIR	7.38E+14	8.18E+13	0.49 ± 0.04
		2.17.99			7.30E+14	8.68E+13	0.49 ± 0.04
	XYL	3.24.99	20	FTIR	8.22E+14	9.39E+13	0.44 ± 0.03
		3.25.99			8.35E+14	1.11E+14	0.49 ± 0.03
1-butene	TMB	7.12.99	>760,[e] 40% SF_6	TC/GC	2.95E+14	4.82E+12	0.25 ± 0.04
	TMB	4.27.99	>760,[e] 40% SF_6	FTIR/GC	1.51E+15	5.90E+13	0.24 ± 0.04
	TMB	4.28.99	>760,[e] 30% SF_6	FTIR/GC	1.43E+15	6.35E+13	0.27 ± 0.04
	XYL	2.23.99	760	FTIR	7.11E+14	7.45E+13	0.23 ± 0.03
	XYL	2.24.99	60	FTIR	7.32E+14	7.98E+13	0.30 ± 0.04
	XYL	2.25.99	20	FTIR	8.48E+14	9.65E+13	0.26 ± 0.04
trans-2-butene	TMB	7.16.99	>760[e], 70% SF_6	TC/GC	3.10E+14	5.54E+12	0.63 ± 0.09
	TMB	7.14.99	>760[e], 50% SF_6	TC/GC	2.88E+14	4.06E+12	0.52 ± 0.06
	TMB	7.21.99	>760[e], 50% SF_6	TC/GC	2.83E+14	4.70E+12	0.58 ± 0.06
	TMB	7.22.99	>760[e], 30% SF_6	TC/GC	2.35E+14	4.53E+12	0.62 ± 0.09
	TMB	3.31.98	760	FT/GC	1.82E+15	3.00E+13	0.59 ± 0.06
	TMB	4.1.98	760	FT/GC	1.62E+15	1.31E+13	0.72 ± 0.07
	TMB	4.2.98	760	FT/GC	1.23E+15	4.92E+13	0.61 ± 0.08
	TMB	4.21.98	760	FT/GC	1.40E+15	2.68E+13	0.77 ± 0.10
	XYL	2.9.99	760	FTIR	6.54E+14	7.01E+13	0.53 ± 0.07
	XYL	2.10.99	760	FTIR	7.26E+14	7.48E+13	0.58 ± 0.06
	TMB	4.3.98	200	FT/GC	8.80E+14	5.61E+13	0.64 ± 0.08
	TMB	4.16.98	200	FT/GC	1.44E+15	4.51E+13	0.61 ± 0.08
	XYL	2.12.99	60	FTIR	7.19E+14	7.40E+13	0.59 ± 0.08
	XYL	2.15.99	60	FTIR	7.69E+14	7.38E+13	0.59 ± 0.06
2,3-dimethyl-2-butene	XYL	2.11.99	760	FTIR	7.16E+14	7.48E+13	0.99 ± 0.10
	XYL	2.26.99	60	FTIR	7.09E+14	7.54E+13	0.85 ± 0.10
	XYL	3.1.99	20	FTIR	7.77E+14	9.32E+13	1.04 ± 0.10
trans-3-hexene	TMB	2.11.98	760	FT/GC	1.74E+15	9.54E+13	0.50 ± 0.07
	TMB	2.16.98	760	FT/GC	1.03E+15	6.77E+13	0.50 ± 0.10
	TMB	2.18.98	760	FT/GC	6.64E+14	5.54E+13	0.49 ± 0.08
	TMB	3.4.98	760	FT/GC	1.34E+15	6.96E+13	0.35 ± 0.05
	TMB	3.9.98	760	FT/GC	1.10E+15	5.61E+13	0.44 ± 0.06
	TMB	2.26.98	760	TC/GC	2.37E+14	8.02E+12	0.65 ± 0.03
	TMB	3.3.98	760	TC/GC	2.25E+14	1.30E+13	0.61 ± 0.03
	TMB	3.10.98	760	TC/GC	2.39E+14	1.46E+13	0.59 ± 0.03
	TMB	2.24.98	350	FT/GC	1.39E+15	5.15E+13	0.41 ± 0.10
	TMB	2.25.98	350	FT/GC	1.22E+15	5.27E+13	0.41 ± 0.10
	TMB	3.12.98	350	FT/GC	6.03E+14	3.38E+13	0.50 ± 0.03
	TMB	3.13.98	350	FT/GC	1.11E+15	6.26E+13	0.47 ± 0.07
	TMB	3.23.98	200	FT/GC	5.61E+14	7.64E+12	0.53 ± 0.05
	TMB	5.19.98	200	FT/GC	5.93E+14	3.10E+13	0.45 ± 0.05
cyclopentene	TMB	4.22.98	760	FT/GC	6.05E+14	1.30E+13	0.52 ± 0.05
	TMB	4.28.98	760	FT/GC	6.00E+14	1.59E+13	0.55 ± 0.05
	TMB	4.30.98	760	FT/GC	4.92E+14	1.61E+13	0.57 ± 0.07
	TMB	5.4.98	760	FT/GC	6.49E+14	2.73E+13	0.63 ± 0.06
	TMB	5.5.98	760	FT/GC	4.75E+14	1.82E+13	0.65 ± 0.07
	TMB	5.11.98	200	FT/GC	2.51E+14	1.09E+13	0.59 ± 0.04
	TMB	5.13.98	200	FT/GC	1.99E+14	6.33E+12	0.62 ± 0.05
	TMB	5.15.98	200	FT/GC	4.74E+14	2.08E+13	0.56 ± 0.05

[a] FT/GC = Flow tube with GC/FID detection, FTIR = long path FTIR cell, TC/GC = Teflon chamber with GC/FID detection, and FTIR/GC = carried out in FTIR cell, using GC/FID for detection. [b] $[A]_o$= initial alkene concentration. [c] $[T]_o$= initial tracer concentration. [d] All OH yields are on a per molecule of alkene reacted with ozone basis. Uncertainties reported here reflect the full scatter in the experimental data. Systematic uncertainties are discussed in the text. [e] SF_6.

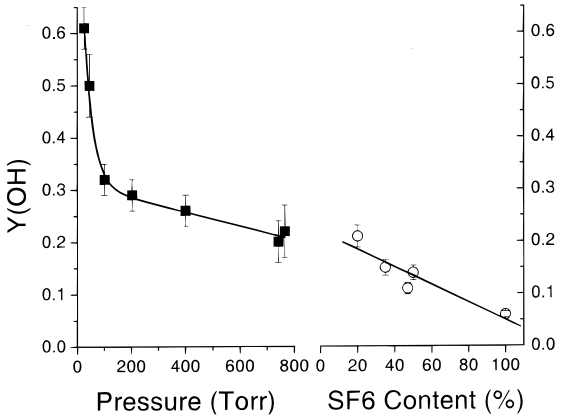

Figure 2. OH formation in ethene ozonolysis as a function of total pressure in air and as a function of SF_6 mixing ratio in air with a total pressure of 1 atm (Table 2). The solid lines are guides only.

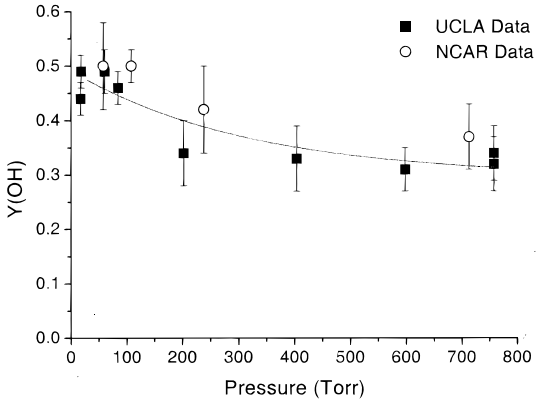

Figure 3. OH formation in propene ozonolysis as a function of total pressure in air. The solid diamonds were acquired in the UCLA FTIR apparatus and the open squares represent data acquired in a similar apparatus at NCAR. The solid line is a simple polynomial fit of the UCLA data.

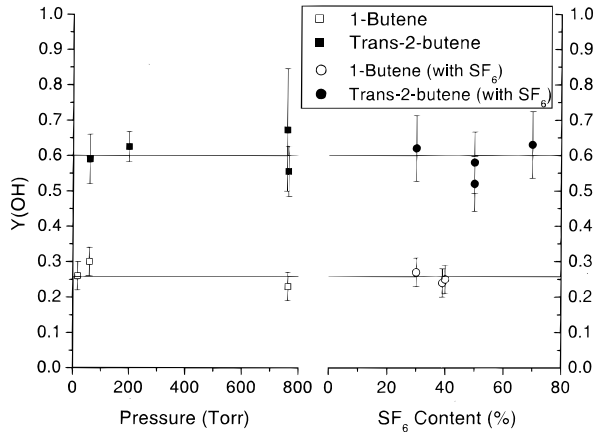

Figure 4. OH formation from 1-butene and *trans*-2-butene ozonolysis as a function of total pressure in air and as a function of SF_6 mixing ratio in air with a total pressure of 1 atm (Table 2). The lines represent the average OH yield over all pressures and SF_6 mixing ratios.

in the presence of added SF_6. Within the uncertainties, no pressure dependence was discernible for any of these higher alkenes.

The experimental formaldehyde yields (per molecule of ethene reacted) and formaldehyde and acetaldehyde yields (per molecule of propene reacted), along with model-generated aldehyde yields, are shown as a function of pressure in Figures 5 and 6. Because aldehydes and alkenes react rapidly with OH

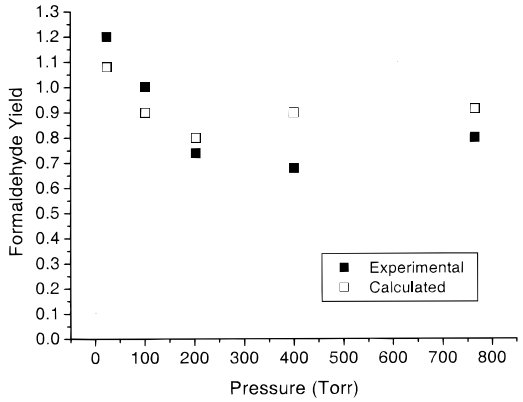

Figure 5. HCHO yields (per molecule of ethene reacted) as a function of pressure. Solid symbols represent experimental data points; open symbols were calculated with the model, assuming a unit yield for HCHO from the ethene−O_3 reaction at all pressures.

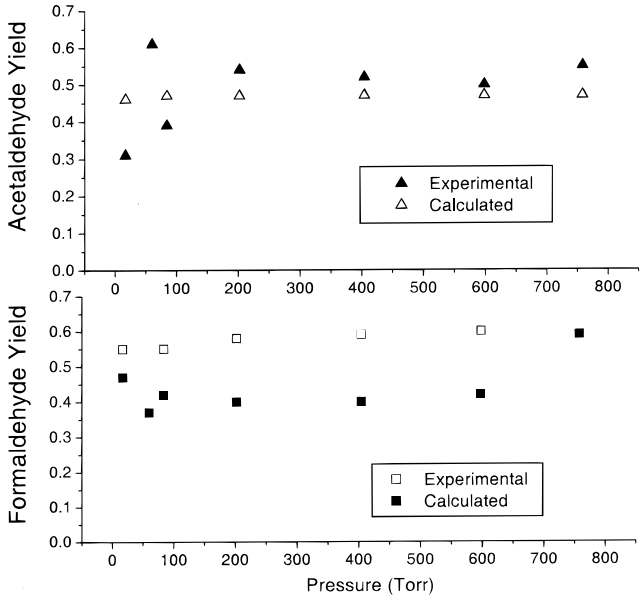

Figure 6. Acetaldehyde and formaldehyde yields (per molecule of propene reacted) as a function of pressure. Solid symbols represent experimental data points; open symbols represent results obtained from the model. Calculated and experimental points at 760 Torr are indistinguishable for formaldehyde.

radicals, an increase in OH radical formation as the pressure is decreased should affect the observed concentration of aldehyde. Assuming a formaldehyde yield of 1.0 for ethene and formaldehyde and acetaldehyde yields of 0.60 and 0.52, respectively, for propene (see Paulson et al.[11] for a full discussion of the propene model) from each molecule of alkene reacted with ozone, we calculated the expected apparent aldehyde yields with respect to *total* alkene reacted (with O_3 and OH, as these experiments did not employ an OH scavenger). This calculation accounts for RO_2-RO_2 and RO_2-HO_2 radical reactions that result from the OH−alkene chemistry (and other sources) but that add uncertainty. Within the uncertainties, the calculations and observations agree, indicating no clear pressure dependence of aldehyde yields. To gain perfect agreement between calculations and observations, the formaldehyde yield from the O_3−ethene reaction needs to be increased from 0.85 at 760 Torr to 1.15 at low pressure.

We also measured the HCHO and CO yields from ethene ozonolysis in the presence of an OH radical scavenger (di-*n*-propyl ether) for the pressure range 50−760 Torr (not shown).

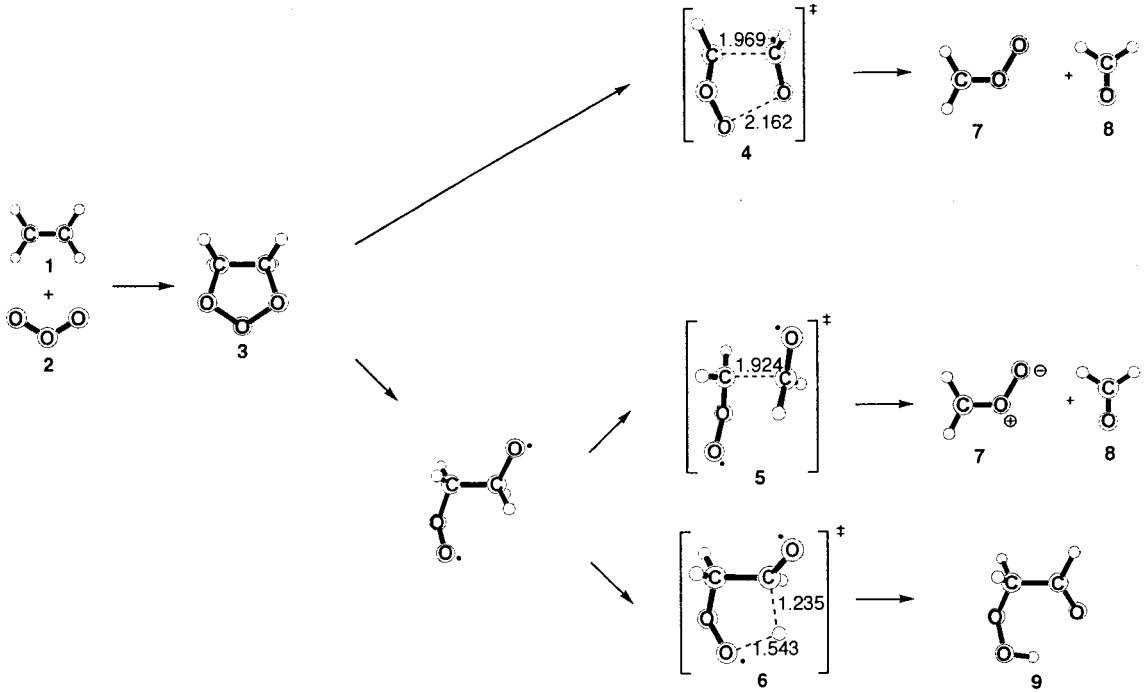

Figure 7. Formation and decomposition of the ethene primary ozonide. Optimized geometries (bond lengths in Å) and relative energies (kcal/mol in Table 3) from (U)B3LYP/6-31G(d,p) calculations.

The average yields obtained from this analysis were 0.86 and 0.35 for HCHO and CO, respectively. Within the precision of the data, there appeared to be no pressure dependence for these yields, although the values at 50 Torr were quite scattered (±60%).

For propene, the absolute agreement between the observed and calculated acetaldehyde and formaldehyde values is good (Figure 6). Neither the observed nor the calculated aldehyde yields show any dependence on pressure.

Thomas et al.[10] measured formation of CO, CO_2, H_2, formic acid, and formaldehyde from ethene ozonolysis at 770, 77, and 7.5 Torr. They observed no differences between 770 and 77 Torr. At 7.5 Torr, they observed an increase in CO and CO_2 and a decrease in the formaldehyde yields, with no change in the H_2 or formic acid yields. Interpretation of these yields is complicated by the high yields of OH at low pressure (Thomas et al.[10] did not use an OH scavenger). Although the Thomas et al.[10] data appear to contradict our formaldehyde yield measurements, it is simply the difference in experimental conditions that affects the apparent formaldehyde yield. Under the conditions used in the Thomas et al.[10] study, the lifetime of OH radicals with respect to reaction with formaldehyde is approximately half the lifetime with respect to reaction with ethene itself; in our experiments, the relative lifetimes are similar so that OH reacts with the tracer as rapidly as it does with formaldehyde. Because of the tracer (which acts to "scavenge" some OH), the increasing OH yield at low pressures does not have as large an effect on the formaldehyde levels in our experiments. The Thomas et al.[10] results are consistent with no strong pressure dependence for the formaldehyde yield. The increase in CO at low pressure is also consistent with a higher OH yield, as CO is a product of formaldehyde oxidation by OH radical. The increase in CO_2 may also be due to an increase in OH, as CO_2 is a common oxidation product as well (from such reactions as OH with aldehydes and with CO).

Carbonyl product yields were quantified from the OH yield experiments for 1-butene, *trans*-2-butene, and 2,3-dimethyl-2-butene as well, in the absence of an OH radical scavenger. We observed no pressure dependence for the carbonyl product yields (per molecule of alkene reacted with O_3 and OH radicals) from 1-butene (0.97 and 1.2 formaldehyde and propionaldehyde, respectively), *trans*-2-butene (1.0 acetaldehyde), and 2,3-dimethyl-2-butene (0.99 acetone).

TABLE 3: Energetics of the Formation and Unimolecular Reactions of the Ethene and Propene Primary Ozonide[a]

	species	ΔE (gas phase)	ΔE (in CH_2Cl_2)
ethene	**1** + **2**	+54.9	
	3	0.0	0.0
	4	+19.2	+16.8
	5	+18.6	+18.3
	6	+16.9	+17.5
	7 + **8**	+5.2	+0.7
	9	−47.6	−48.4
propene	**1** + **2**	+55.9	
	3	0.0	
	4	+17.8	
	5	+16.2	
	6	+16.0	
	7 + **8**	+0.4	
	9	−45.9	

[a] Relative energies in kcal/mol. Species labeled in Figure 7.

Figure 7 and Table 3 summarize our UB3LYP/6-31G(d,p) model of ethene ozonolysis. After its exothermic formation (ΔE = −54.9 kcal/mol), the chemically activated primary ozonide (**3**) may decompose by either concerted or stepwise diradical pathways. The concerted cycloreversion of the ozonide (**4**) has an activation barrier of 19.2 kcal/mol; the formation of the parent carbonyl oxide (**7**) and formaldehyde (**8**) is endothermic by 5.2 kcal/mol. Alternatively, the primary ozonide may decompose by the initial formation of an oxy/peroxy diradical intermediate (Figure 8), which then undergoes further reaction (Figure 7, **5** and **6**). Although diradical formation is initiated by a simple homolysis of an O−O bond, there is nevertheless a transition structure for this process 12.8 kcal/mol above the primary

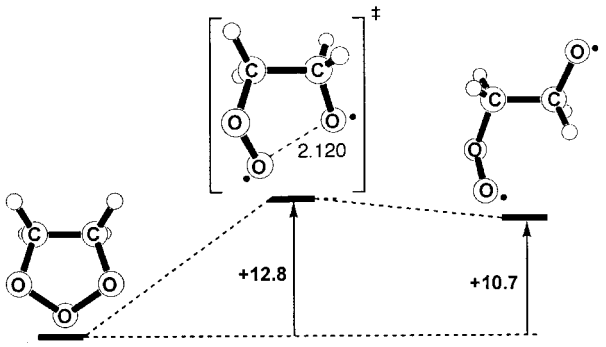

Figure 8. Formation of the anti oxy/peroxy diradical from the ethene primary ozonide. Relative energies (kcal/mol) and geometries of reactant, transition structure (bond length in Å), and product from (U)B3LYP/6-31G(d,p) calculations.

ozonide. The lowest-energy conformation of the diradical intermediate is 10.7 kcal/mol above the ozonide.

The transition structure (Figure 7, **5**) for the fragmentation of the diradical to give the parent carbonyl oxide and formaldehyde is 18.6 kcal/mol above the primary ozonide. The stepwise Criegee mechanism is therefore predicted to be kinetically favored by 0.6 kcal/mol over the concerted Criegee mechanism. The cleavage of the C−C bond in the diradicaloid transition structure is slightly less advanced than C−C bond cleavage in the closed-shell transition structure (1.924 Å vs. 1.969 Å).

Alternatively, the diradical intermediate can isomerize to form hydroperoxyacetaldehyde (Figure 7, **9**). The 1,4-hydrogen shift transition structure (Figure 7, **6**) is predicted by our UB3LYP/6-31G(d,p) calculations to be only 16.9 kcal/mol above the primary ozonide, about 2 kcal/mol lower than formation of the Criegee intermediate by either diradical or closed-shell pathways. The formation of the hydroperoxide is therefore predicted to be the fastest process in gas-phase ethene ozonolysis.

The experimental consensus is that solution-phase ozonolysis proceeds by a concerted mechanism.[43] We have therefore studied the effect of solvation by dichloromethane on the ethene ozonolysis reaction. Single-point SCIPCM calculations on the UB3LYP/6-31G(d,p) stationary points reveal that the concerted cycloreversion of the primary ozonide—that is, the traditional Criegee mechanism—becomes the lowest barrier process by 0.7−1.5 kcal/mol in solution (Table 3). This is qualitatively reasonable, as the cycloreversion transition structure ($\mu = 4.56$ D) is far more polar than either the 1,4-hydrogen shift ($\mu =$ 1.73 D) or the diradical cleavage ($\mu = 1.49$ D) transition structures.

Formation of hydroperoxyacetaldehyde is highly exothermic ($\Delta E = -47.6$ kcal/mol), and this species will likely undergo further unimolecular reaction (Figure 9). Cleavage of the peroxy bond to afford hydroxyl radical requires 40.7 kcal/mol. The cogenerated acetaldehyde alkoxy radical will then readily cleave to give formaldehyde and the formyl radical.

Figure 10 and Table 3 summarize our predictions for propene ozonolysis. The asymmetry of the propene primary ozonide gives rise to four possible cycloreversion channels. For simplicity, we show only the results for the concerted pathway leading to the syn carbonyl oxide (the major OH formation channel), along with the analogous diradical channel. Like ethene, the primary ozonide of propene (**3**) may decompose by either concerted or stepwise diradical pathways. The concerted cycloreversion of the ozonide (**4**) to give syn acetaldehyde oxide has an activation barrier of 17.8 kcal/mol and a reaction energy of 0.4 kcal/mol. The primary ozonide may also decompose through the intermediacy of an oxy/peroxy diradical. The most stable diradical intermediate is 10.4 kcal/mol above the primary ozonide. The stepwise formation of syn acetaldehyde oxide (that is, by cleavage of the diradical intermediate) has an activation barrier of 16.2 kcal/mol (**5**). The diradicaloid pathway is kinetically favored over the concerted pathway by 1.6 kcal/mol.

Formation of 2-hydroperoxypropanal (**9**) through a 1,4-hydrogen shift transition structure (**6**) has an activation barrier of 16.0 kcal/mol. The formation of the Criegee intermediate and the hydroperoxide should therefore occur at nearly equal rates in gas-phase propene ozonolysis.

The unimolecular reactions of the ethene and propene primary ozonides all have slightly positive activation entropies. The diradical cleavage transition states are the most favored entropically, with $\Delta S^{\mp}$ values of 5−6 cal/(mol K); thus, stepwise formation of carbonyl oxides should become slightly more favorable with increasing temperature. The other transition states have $\Delta S^{\mp}$ values of 1−2 cal/(mol K).

Discussion

Theoretical work by Olzmann et al.[19] addressed the pressure dependence of OH radical yield from the ozonolysis of ethene and 2,3-dimethyl-2-butene. Using master-equation analysis, they predicted that the OH radical yield from ethene ozonolysis would be ∼0.002 and would be independent of pressure. As a possible explanation for the discrepancy between their value and the experimental values available, they proposed that a diradical pathway could explain the additional OH formed in experiments, as they only took into account the traditional Criegee mechanism for OH radical formation (R1a and R2). In this same study, they predict that the OH radical yield from 2,3-dimethyl-2-butene ozonolysis would be pressure dependent, increasing from ∼0.7 at atmospheric pressure to ∼0.9 at 7.5 Torr.

Hatakeyama et al.'s studies of thermalized carbonyl oxide formation[17,18] found a dependence on pressure for the quantity formed in both ethene and *trans*-2-butene ozonolysis. The pressure dependence of the carbonyl oxide is not necessarily linked to that of the OH yield, however. Because there are several isomerization channels open to carbonyl oxides (and the ozonide itself), there need not be a direct correlation between thermalized carbonyl oxides and OH yield, other than the requirement that the combined yields not exceed 1.[16] When the thermalized carbonyl oxide yield decreases at low pressure, the OH formation channel may increase (as in ethene) or another channel may increase (possibly dioxirane formation), resulting in no effect on the OH yield (as in *trans*-2-butene). Another consideration is that the Hatakeyama et al. studies[17,18] assume that all thermalized carbonyl oxides react bimolecularly, and recent theoretical work suggests that this may not be the case. Olzmann et al.[19] calculated that, even for completely thermalized carbonyl oxides, the high-pressure limiting rate coefficients for unimolecular decomposition give lifetimes of only 3 s for CH_2-OO and 0.004 s for CH_3CHOO, and suggested that these values are upper limits. Hatakeyama et al.[17] noted that, at atmospheric pressure, the propene ozonide was observed for ozonolysis of ethene in the presence of excess acetaldehyde, but at low pressures (∼55 Torr), none of the secondary ozonide was observed. This may indicate either decomposition of the secondary ozonide or decomposition of the thermalized carbonyl oxide itself competing with reaction with aldehyde more efficiently at low pressure.

For these highly complex ozonolysis reactions, several explanations of pressure dependence and its apparent relation-

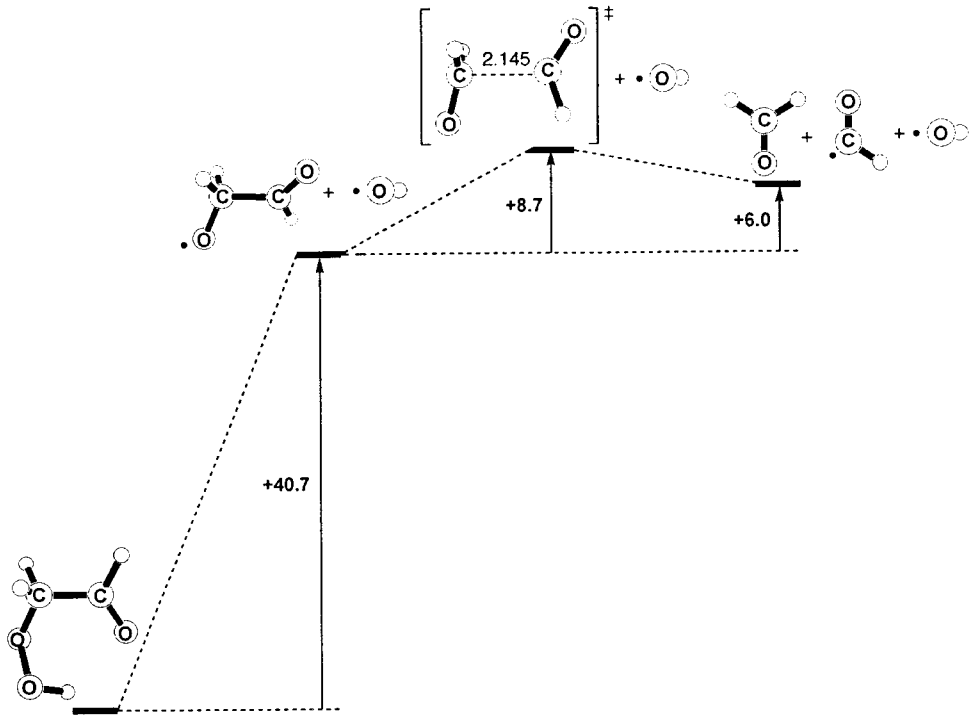

Figure 9. Decomposition of hydroperoxyacetaldehyde. Relative energies (kcal/mol) and geometries of reactant, transition structure (bond length in Å), and products from (U)B3LYP/6-31G(d,p) calculations.

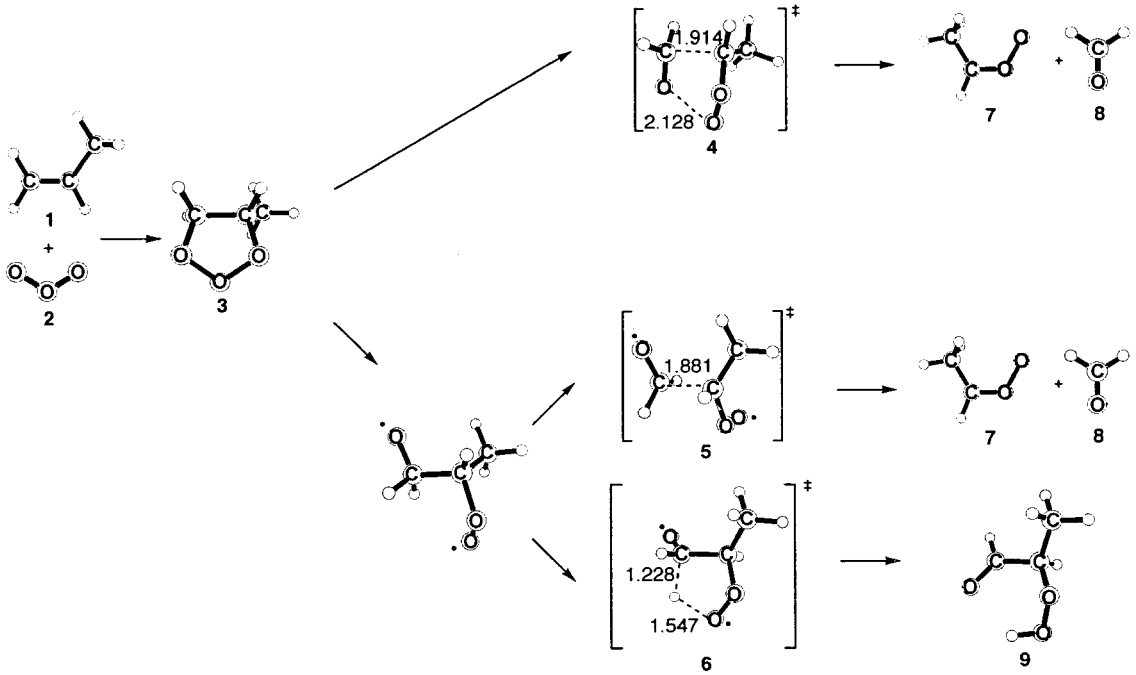

Figure 10. Formation and decomposition of the propene primary ozonide. Optimized geometries (bond lengths in Å) and relative energies (kcal/mol in Table 3) from (U)B3LYP/6-31G(d,p) calculations.

ship to chain length for 1-alkenes are possible. It is unlikely that variation in formation of CH_2OO is responsible, as the aldehyde coproduct has a yield of about 50% for the series of terminal alkenes $>C_3$ at all pressures studied. Similarly, it seems unlikely that yields of syn and anti carbonyl oxides would change appreciably with pressure. Another, more plausible, explanation relies on energy partitioning when the primary ozonide decomposes. Assuming a statistical distribution of energy, as the alkyl chain length increases, the fraction of energy partitioned to the CH_2OO fragment will decrease. For the CH_2OO carbonyl oxide, the energy barrier to OH formation is ∼31 kcal/mol, and that for dioxirane formation is ∼18 kcal/mol (although the transition state for OH formation is loose, which makes this pathway somewhat more favorable than the energy barriers suggest).[24] Thus, as the CH_2OO is formed with less and less energy, it may eventually reach a point at which it is unable to form OH. This explanation is problematic, however. On the basis of ab initio calculations for OH formation from CH_2OO, it is difficult to rationalize an OH yield of 0.2 for ethene, let alone 0.6.[5,19] Furthermore, if OH from CH_2OO is pressure-dependent, OH from the substituted carbonyl oxide might be pressure- dependent as well, particularly because it

has a higher density of vibrational states and would thus presumably be more easily collisionally deactivated at higher pressures.[19]

Our calculations suggest that an alternative to the Criegee mechanism, the diradical pathway, may be important for ethene and propene at low pressure. The ethene pressure-dependence data are consistent with the preferential formation of hydroperoxyacetaldehyde predicted by our B3LYP calculations. Activation entropies slightly favor the diradical cleavage pathway over the 1,4-hydrogen shift pathway. However, an RRKM calculation is required to quantify the competition between enthalpy and entropy for the vibrationally excited primary ozonide.

At low pressures, the chemically activated hydroperoxide should largely decompose to give OH radical. Although the homolysis of the peroxy bond requires 41 kcal/mol, the overall transformation from the primary ozonide to OH radicals via the hydroperoxide is exothermic by 7 kcal/mol. The primary ozonide is initially formed with more than enough energy to surmount this 41 kcal/mol barrier, but it seems reasonable to assume that, with a barrier of this magnitude, collisional deactivation may compete with OH formation from this channel. Moreover, as Figure 9 shows, the decomposition of hydroperoxyacetaldehyde should generate equal amounts of OH and formaldehyde. This is consistent with our low-pressure aldehyde data.

Our SCIPCM calculations (Table 3) indicate that the polarity of the cycloreversion transition structure is sufficient to favor the Criegee mechanism even in a solvent of modest dielectric moment like dichloromethane ($\epsilon = 8.93$). Our predictions that hydroperoxyacetaldehyde is the key intermediate in gas-phase ethene ozonolysis does not contradict the extensive experimental evidence for the dominance of the Criegee mechanism in solution-phase ozonolysis.[43]

Our B3LYP predictions are qualitatively different from the ab initio predictions of Anglada et al.[25] Their CCSD(T) calculations indicate that the concerted cycloreversion transition state (Figure 7, **4**) is lower in energy than the transition state for rearrangment to the hydroperoxide (Figure 7, **6**) by 4.1 kcal/mol, and they conclude that formation and decomposition of the hydroperoxide can play only a minor role in ethene ozonolysis. These theoretical predictions are not consistent with OH yields of >30% below 100 Torr. It would appear that unrestricted density functional theory makes predictions about ethene ozonolysis that are more consistent with the current experimental results.[53]

One unresolved problem with our theoretical model concerns the fate of the hydroperoxide at higher pressures. Under such conditions, hydroperoxyacetaldehyde would be collisionally stabilized against homolysis of the O−O bond and production of OH, a process that is enthalpically demanding (Figure 9) but entropically favorable. This is consistent with experiment. However, hydroperoxyacetaldehyde has never been detected in ethene ozonolysis experiments. Moreover, the yield of formaldehyde from the ethene−ozone reaction has been measured to be close to unity over a wide range of pressures (Figure 5). Our theoretical model cannot account for production of formaldehyde from the collisionally stabilized hydroperoxide. If our model is correct, there must exist a low-barrier pathway for the unimolecular decomposition of hydroperoxyacetaldehyde to give formaldehyde without concomitant production of OH. The putative rate-limiting step of such a mechanism would have an activation enthalpy of less than 41 kcal/mol and a small activation entropy. Calculations in progress seek to discover such a mechanism.

Alternatively, our diradical proposal could be incorrect, and the traditional Criegee mechanism is fully valid even for ethene. Judging from the quantum chemical predictions of Gutbrod et al.,[24] the Criegee intermediate will primarily close to the dioxirane. The formic acid formed from the dioxirane (R2b) could then serve as the pressure-dependent source of OH. Although homolysis of the C−O bond in HCOOH is not the lowest-barrier pathway,[52] this entropically favored pathway could dominate at low pressures.

For propene ozonolysis, the diradical cleavage transition state is of nearly the same energy as the 1,4-hydrogen shift transition state (Table 3). As in ethene ozonolysis, the diradical pathways are predicted to be favored over the concerted cycloreversion transition states. Our B3LYP calculations predict, however, that a smaller fraction of the hydroperoxy aldehyde will be formed. This is consistent with our experimental results, which indicate that the OH yield from propene ozonolysis depends less on the pressure than does that from ethene.

It is likely that the pressure dependence of the species studied here will be of minor importance in the atmosphere. Because of the short lifetime of alkenes in the atmosphere (seconds to hours[14] for 2,3-dimethyl-2-butene and ethene, respectively) transport out of the troposphere, to regions where pressures drop below 100 Torr, is negligible.[14]

Acknowledgment. We thank the National Science Foundation (ATM-9629577 and CHE-9616772) and the Environmental Protection Agency for financial support of this work. Computational work was made possible by the UCLA Office of Academic Computing, the National Center for Supercomputing Applications, and the National Partnership for Advanced Computational Infrastructure. S.E.P. thanks Drs. J. Orlando and G. Tyndall for assistance with the experiments performed at the National Center for Atmospheric Research and Prof. G. Barney Ellison at the University of Colorado for providing a pure sample of 1,3,5-TMB in Boulder on short notice.

References and Notes

(1) Niki, H.; Maker, P. D.; Savage, C. M.; Breitenback, L. P.; Hurley, M. D. *J. Am. Chem. Soc.* **1987**, *91*, 941−946.

(2) Atkinson, R.; Aschmann, S. M.; Arey, J.; Shorees, B. *J. Geophys. Res.* **1992**, *97*, 6065−6073.

(3) Paulson, S. E.; Flagan, R. C.; Seinfeld, J. H. *Int. J. Chem. Kinet.* **1992**, *24*, 79−102.

(4) Atkinson, R.; Aschmann, S. M. *Environ. Sci. Technol.* **1993**, *27*, 1357−1363.

(5) Donahue, N. M.; Kroll, J. H.; Anderson, J. G.; Demerjian, K. L. *Geophys. Res. Lett.* **1997**, *25*, 59−62.

(6) Paulson, S. E.; Sen, A. D.; Liu, P.; Fenske, J. D.; Fox, M. J. *Geophys. Res. Lett.* **1997**, *24*, 3193−3196.

(7) Gutbrod, R.; Kraka, E.; Schindler, R. N.; Cremer, D. *J. Am. Chem. Soc.* **1997**, *119*, 7330−7342.

(8) Paulson, S. E.; Orlando, J. J. *Geophys. Res. Lett.* **1996**, *23*, 3727−3730.

(9) Paulson, S. E.; Chung, M.; Sen, A. D.; Orzechowska, G. *J. Geophys. Res.* **1998**, *103*, 25533−25539.

(10) Thomas, W. F.; Zabel, F.; Becker, K. H.; Fink, E. H. In *Physio-Chemical Behaviour of Atmospheric Pollutants*; Commission of the European Communities: Varese, Italy, 1993; pp 207−212.

(11) Paulson, S. E.; Fenske, J. D.; Sen, A. D.; Callahan, T. W. *J. Phys. Chem. A* **1999**, *103*, 2050−2059.

(12) Harding, L. B.; Goddard, W. A. *J. Am. Chem. Soc.* **1978**, *100*, 7180−7188.

(13) Wadt, W. R.; Goddard, W. A. *J. Am. Chem. Soc.* **1975**, *97*, 3004−3021.

(14) Finlayson-Pitts, B. J.; Pitts, J. *Atmospheric Chemistry: Fundamentals and Experimental Techniques*; Wiley: New York, 1986.

(15) Atkinson, R. *J. Phys. Chem. Ref. Data* **1997**, *26*, 215−290.
(16) Paulson, S. E.; Chung, M.; Hasson, A. *J. Phys. Chem. A* **1999**, *103*, 8125−8138.
(17) Hatakeyama, S.; Kobayashi, H.; Lin, Z.-Y.; Takagi, H.; Akimoto, H. *J. Phys. Chem.* **1986**, *90*, 4131−4135.
(18) Hatakeyama, S.; Kobayashi, H.; Akimoto, H. *J. Phys. Chem.* **1984**, *88*, 4736−4739.
(19) Olzmann, M.; Kraka, E.; Cremer, D.; Gutbrod, R. Anderson, S. *J. Phys. Chem. A* **1997**, *101*, 9421−9429.
(20) O'Neal, H. E.; Blumstein, C. *Int. J. Chem. Kinet.* **1973**, *5*, 397−413.
(21) Cremer, D. *J. Am. Chem. Soc.* **1981**, *103*, 3619−3626.
(22) Dewar, M. J. S.; Hwang, J. C.; Kuhn, D. R. *J. Am. Chem. Soc.* **1991**, *113*, 735−741.
(23) Anglada, J. M.; Bofill, J. M.; Olivella, S.; Sole, A. *J. Am. Chem. Soc.* **1996**, *118*, 4636−4647.
(24) Gutbrod, R.; Schindler, R. N.; Kraka, E. Cremer, D. *Chem. Phys. Lett.* **1996**, *252*, 221−229.
(25) Anglada, J. M.; Crehuet, R.; Bofill, J. M. *Chem. Eur. J.* **1999**, *5*, 1809−1822.
(26) Atkinson, R. J. *J. Phys. Chem. Ref. Data* **1994**, Monograph 2, 1−216.
(27) Kramp, F.; Paulson, S. E. *J. Phys. Chem. A* **1998**, *102*, 2685−2690.
(28) Jenkin, M. E.; Hayman, G. D. *J. Chem. Soc., Faraday Trans.* **1995**, *91*, 1911−1922.
(29) Lightfoot, P. D.; Cox, R. A.; Crowley, J. N.; Destriau, M.; Hayman, G. D.; Jenkin, M. E.; Moortgat, G. K.; Zabel, F. *Atmos. Environ.* **1992**, *26A*, 1805−1961.
(30) DeMore, W. B.; Sander, S. P.; Howard, C. J.; Ravishankara, A. R.; Golden, D. M.; Kolb, C. E.; Hampson, R. F.; Kurylo, M. J.; Molina, M. J. *Chemical Kinetics and Photochemical Data for Use in Stratospheric Modeling−Evaluation Number 12*; Publication 97-4; Jet Propulsion Laboratory: Pasadena, CA, 1997.
(31) Klein, T.; Barnes, I.; Becker, K. H.; Fink, E. H.; Zabel, F. *J. Phys. Chem.* **1984**, *88*, 5020−5025.
(32) Atkinson, R. *Chem. Rev.* **1985**, *85*, 69−201.
(33) Atkinson, R. *J. Phys. Chem. Ref. Data* **1989**, Monograph 1, 1.
(34) Shetter, R. E.; Davidson, J. A.; Cantrell, C. A.; Calvert, J. G. *Rev. Sci. Instrum.* **1987**, *58*, 1427−1428.
(35) Becke, A. D. *J. Chem. Phys.* **1993**, *98*, 5648−5652.
(36) Hehre, W. J.; Ditchfield, R.; Pople, J. A. *J. Chem. Phys.* **1972**, *56*, 2257−2261.
(37) Hariharan, P. C.; Pople, J. A. *Theor. Chim. Acta* **1973**, *28*, 213−222.
(38) Frisch, M. J.; Trucks, G. W.; Schlegel, H. B.; Gill, P. M. W.; Johnson, B. G.; Robb, M. A.; Cheeseman, J. R.; Keith, T.; Petersson, G. A.; Montgomery, J. A.; Raghavachari, K.; Al-Laham, M. A.; Zakrzewski, V. G.; Ortiz, J. V.; Foresman, J. B.; Cioslowski, J.; Stefanov, B. B.; Nanayakkara, A.; Challacombe, M.; Peng, C. Y.; Ayala, P. Y.; Chen, W.; Wong, M. W. Andres, J. O.; Replogle, E. S.; Gomperts, R.; Martin, R. L.; Fox, D. J.; Binkley, J. S.; Defrees, D. J.; Baker, J.; Stewart, J. P.; Head-Gordon, M.; Gonzalez, C.; Pople, J. A. *Gaussian 94*, Revision B.2; Gaussian Inc.: Pittsburgh, PA, 1995.
(39) Frisch, M. J.; Trucks, G. W.; Schlegel, H. B.; Scuseria, G. E.; Robb, M. A.; Cheeseman, J. R.; Zakrzewski, V. J.; Montgomery, J. A., Jr.; Strapmann, R. E.; Burant, J. C.; Dapprich, S.; Millam, J. M.; Daniels, A. D.;Kudin, K. N.; Strain, M. C.; Farkas, O.; Tomasi, J.; Barone, V.; Cossi, M.; Cammi, R.; Mannucci, B.; Pomelli, C.; Adamo, C.; Clifford, S.; Ochterski, J.; Petersson, G. A.; Ayala, P. Y.; Cui, Q.; Morokuma, K.; Malick, D. K.;Rabuck, A. D.; Raghavachari, K.; Foresman, J. B.; Cioslowski, J.; Ortiz, J. V.; Stefanov, B. B.; Liu, G.; Liashenko, A.; Piskorz, P.; Komaromi, I.; Gomperts, R.; Martin, R. L.; Fox, D. J.; Keith, T.; Al-Laham, M. A.; Peng, C. Y.; Nanayakkara, A.; Gonzalez, C.; Challacombe, M.; Gill, P. M. W.; Johnson, B. G.; Chen, W. Wong, M. W.; Andres, J. L.; Head-Gordon, M.; Replogle, E. S.; Pople, J. A. *Gaussian 98*, Revision A.6; Gaussian, Inc.: Pittsburgh, PA, 1998.
(40) Grosjean, D.; Friedlander, S. K. *Formation of Organic Aerosols from Cyclic Olefins and Di-olefins*. In *Character and Origins of Smog Aerosols*; Hidy, G. M., Ed.; Wiley: New York, 1979; p 435−473.
(41) Pandis, S. N.; Harley, R. H.; Cass, G. R.; Seinfeld, J. H. *Atmos. Environ.* **1992**, *27A*, 2403−2416.
(42) Miller, L. A.; Barker, J. R. *J. Chem. Phys.* **1996**, *105*, 1383−1391.
(43) Bailey, P. S. *Ozonation in Organic Chemistry*; Academic Press: New York, 1982; Vol. 2.
(44) Wilsey, S.; Bernardi, F.; Olivucci, M.; Robb, M. A.; Murphy, S.; Adam, W. *J. Phys. Chem. A* **1999**, *103*, 1669−1677.
(45) Rickard, A. R.; Johnson, D.; McGill, C. D.; Marston, G. *J. Phys. Chem. A* **1999**, *103*, 7656−7664.
(46) Gutbrod, R.; Meyer, S.; Rahman, M. M.; Schindler, R. N. *Int. J. Chem. Kinet.* **1997**, *29*, 717−723.
(47) Mihelcic, D.; Heitlinger, M.; Kley, D.; Musgen, P.; Volz-Thomas, A. *Chem. Phys. Lett.* **1999**, *301*, 559−64.
(48) Neeb, P.; Moortgat, G. K. *J. Phys. Chem.* **1999**, *103*, 9003−9012.
(49) Orzechowska, G. E.; Paulson, S. E., research in progress.
(50) McGill, C.; Rickard, A.; Johnson, D.; Marston, G. *Chemosphere* **1999**, *38*, 1205−1212.
(51) Chew, A. A.; Atkinson, R. *J. Geophys. Res.* **1996**, *101*, 28649−28653.
(52) Fenske, J. D.; Kuwata, K. T.; Houk, K. N.; Paulson, S. E. *J. Phys. Chem. A* **2000**, *104*, in press.

(53) Although high-level methods were used to compute the single-point energies, they may nevertheless be inadequate. The CCSD(T) method can be expected to be unreliable in treating systems with significant diradical character. Although CASPT2 is an excellent method for simultaneous treatment of static and dynamic electron correlation in diradicals, large active spaces are often required. Agreement between the experimental and CASPT2 activation barriers for the thermal decomposition of 1,2-dioxetane required use of a (12, 10) active space.[44] The analogous space for the ethene primary ozonide, including the relevant σ/σ^* (C−H) orbitals, would be (20, 17), far larger than the (6, 6) space employed by Anglada et al.[25]